Corruption of Radio Metric Doppler Due to Solar Plasma Dynamics: S/X Dual-Frequency Doppler Calibration for These Effects

F. B. Winn, S. R. Reinbold, K. W. Yip, and R. E. Koch
Tracking and Orbit Determination Section
A. Lubeley
Mission Computing Section

The quality of DSN radio metric doppler, for spacecraft beyond a distance of 1 AU from Earth, is a strong function of the Sun–Earth–probe angle. The rms noise levels of both S- and X-band doppler for Sun–Earth–probe angle < 20 deg are observed to be orders of magnitude greater than nominal. Mariner 6, 7, 9, and 10 and Pioneer 10 and 11 doppler data are discussed and the rms noise level for various Sun–Earth–probe angles are shown. Such solar plasma-related doppler degradation reduced the Mariner 10–Mercury II encounter navigation accuracy by nearly a factor of 10. Furthermore, this degradation is shown to be indirectly related to plasma dynamics and not a direct measure of the dynamics.

I. Doppler RMS Noise Dependence on Sun–Earth–Probe angle

For spacecraft beyond 1 AU from Earth, radio metric doppler rms noise is observed to be a predominant function of the angular separation of the probe and the Sun as seen from Earth.

The positions and velocities of a spacecraft in the solar system are estimated usually by a least squares, differential correction technique (Orbit Determination Program, Ref. 1). The doppler shift experienced by round-trip radio transmission from Earth to the spacecraft and back is the prime observable used in the least squares technique. A part of the procedure computes the difference between the observed doppler shift and the doppler shift computed from numerical integrations of the equations of motion of all the significant solar system bodies.

The rms noise for each deep space station–spacecraft view period is computed:

$$\frac{1}{N}\left\{\sum^{N}(O-C)^2-\left(\sum^{N}(O-C)\right)^2\right\}^{1/2} \qquad (1)$$

where

$N \equiv$ number of observations that exist for a given tracking pass after the obvious "blunder observations" have been removed from consideration.

$O \equiv$ observed doppler shift

$C \equiv$ computed doppler shift

Figure 1 shows Mariner 9 and 10 and Pioneer 10 and 11 rms doppler noise levels (for each pass) for a range of Sun–Earth–probe (SEP) angles.

The Orbit Determination Program (ODP) does not utilize any model to account for the plasma corruptions of doppler. No model of sufficient accuracy exists at this time. Typically, empirical measurements (differenced range versus integrated doppler (DRVID), Ref. 2) are used to provide information concerning the long-term fluctuations of the plasma. Plasma dynamics of short time durations (< 1 second) are not recorded by DRVID. Yet, it is these high-frequency dynamics which yield the phase jitter, the rms doppler noise shown in Fig. 1.

Muhleman (Ref. 3) notes that the rms phase jitter is dependent on the observing wavelength and the line-of-sight electron content fluctuation. He further notes that for space regions beyond 5 solar radii the electron density fluctuation is approximately proportional to the mean plasma density. Assuming these observations hold for all solar distances, he predicted rms doppler noise levels for $|SEP| < 90$ deg (Fig. 1).

Although, in general, the maximum rms noise occurs at $SEP = 0$ deg and diminishes rapidly with increased SEP angle, there are localized fluctuations which change the noise levels of 2 to 10 times in many cases. They are most clearly resolved in the Mariner Venus–Mercury (MVM'73) noise plot.

Additionally, as one might expect, the amplitude and temporal variations of the rms phase jitter are different for each mission: This long-term variability is most likely tied to the amount of solar activity. Indeed, studies by MacDoran (Ref. 2) and Berman (Ref. 4) have shown that a relationship between the two does exist. Although these studies are encouraging, there is no way to predict the amount of doppler phase jitter that will result at a particular point in space and at an instant in time.

II. Doppler Noise Characteristics

Plasma-corrupted doppler differs from nominal doppler in two ways: (1) increased phase jitter or high-frequency noise, and (2) occasional to frequent doppler phase discontinuities (cycle slips).

Increased rms noise of plasma-influenced doppler is apparent in Fig. 2. Esposito (Ref. 5) originally presented this figure. There are occasions of plasma-corrupted data shown here at SEP angles > 20 deg. And all doppler acquired at $|SEP| < 10$ deg has been so affected. These doppler sets were acquired from the Mariner 6 and 7 spacecraft in 1969, a year in which the Sun activity was at minimum.

With an increased resolution in time, Fig. 3 shows nominal and plasma-corrupted doppler residuals. A doppler residual is defined as the difference between the doppler shift observed (O in Eq. 1) and the doppler shift computed using the ODP mathematical model (C in Eq. 1). Figures 3a through e show doppler residuals for the Pioneer spacecraft. The lower a frame appears in the sequence, the smaller the associated SEP angle. All of the Pioneer doppler have been averaged over a 60-s count time.

Figures 3a and b are good examples of nominal doppler residuals and corrupted residuals. During the first two hours of those passes of tracking data, nominal doppler noise is apparent. Each of these nominal periods is followed by time periods in which the doppler residual noise increases 5 to 10 times. In addition, short-term temporal variations appear in the doppler residuals that are not present in the nominal doppler residuals.

There is no assurance that these signatures and/or the phase jitter (high-frequency variation) are due to solar plasma concentrations, especially for such large SEP angles: $SEP \approx 130$ deg for Fig. 3a and $SEP \approx 100$ deg for Fig. 3b. However, note the similarity between the Pioneer doppler residuals acquired at $SEP \approx 130$ and 12 deg. The residuals in Fig. 3a show monotonic frequency changes over time scales of tens of minutes. There is a series of them during the fifth and seventh hours of this tracking period. A very similar behavior is evident in Fig. 3d, which shows residuals associated with an SEP angle of 12 deg. And, of course, there is the excessive phase jitter noise.

III. Correlated Noise Events of Different Spacecraft

These doppler residual noise patterns are thought to be the result of plasma fluctuations. This contention is supported by observations that both the noise (Fig. 1) and the time duration of the disturbances (Fig. 4) decrease as the SEP angle increases. Additionally, it is interesting to note that P. S. Callahan, A. J. Anderson, and G. W. Null, and the authors have succeeded in correlating doppler "noise bursts" believed to be plasma-related seen along the Pioneer 10 line-of-sight with those seen along the Pioneer 11 line-of-sight a day later. Figure 5 shows one such correlated event/set discovered by Null.

IV. The Dispersive Nature of Charged-Particle Dynamics

If, indeed, the doppler noise dependence on SEP angle and time stems from plasma dynamics only, then dual-frequency doppler observations can be used to compute the plasma fluctuations which occur along the raypath during any continuous observation period. Theory and observations (Ref. 6) show

$$\Delta\ell = -\frac{e^2}{2\varepsilon_0 m\omega^2}\int N(\ell)\, d\ell \qquad (2)$$

where

e = electron charge

m = electron mass

ε = electric permitivity of free space

ω = frequency of propagation

N = electron density at ℓ

V. Dual-Frequency Charged-Particle Calibration Experience

The Mariner Venus–Mercury 1973 mission was the first to use both S- and X-band frequency doppler to derive charged-particle calibrations in a navigation application. Basically, the system functioned in the following manner:

(1) An S-band frequency ($\sim$ 2100 MHz) was transmitted from a DSN station to the Mariner 10 spacecraft.

(2) The spacecraft in turn retransmitted the received S-band frequency after multiplication of the received signal by 240/221.

(3) The spacecraft simultaneously multiplied the received signal by 880/221 (a factor of 11/3 greater than 240/221) and retransmitted the signal to the ground station.

Thus, on the spacecraft-to-ground station downleg path, dual S/X frequency radio propagations were transmitted.

This dual-frequency system was possible because the spacecraft had both S- and X-band transmitters and G. Levy and others equipped the Mars Station (DSS 14) at Goldstone, California with an experimental X-band receiver. DSS 14 was the only deep space station so equipped.

In practice, the time histories of the DSS 14 S- and X-band phase over a tracking interval were differenced as follows:

$$\Delta\phi = 1.02\left(\phi_s - \frac{3}{11}\phi_x\right) \qquad (3)$$

where ϕ_s, ϕ_x are the accumulated phase changes of the S- and X-band carriers from the start of the tracking interval. Both phase time histories show the radial velocity of spacecraft relative to the station, but this will be differenced out in Eq. (3), leaving the charged-particle dynamics information.

The factor 1.02 accounts for the fact that the X-band phase delay due to charged-particle dynamics is not zero, but $(3/11)^2$ of the S-band phase delay resulting from charged-particle dynamics.

The S/X dual-frequency doppler technique appears to have functioned as expected for the approach navigation of Mariner 10 for the first encounter with Mercury (Ref. 7).

In the 13 days just before the encounter (March 16 to March 29, 1974), the doppler tracking data on 6 of these days (Fig. 6) showed abnormally high-frequency noise (10–20 MHz peak-to-peak amplitude) and over periods of hours. During this time period the SEP angle was $\approx$ 34 deg.

S/X dual-frequency doppler data were used (near-real-time) to identify solar plasma dynamics as the source of

the increased doppler noise: later, as a demonstration, the calibrations were applied to the affected doppler (for which calibrations existed) to show that the calibrations:

(1) Improved the accuracy of the navigation by 80%, reducing the navigation error at Mercury by almost 500 km.

(2) Improved the quality of the data "fit," removing much of the plasma signatures from the residuals as shown in Figs. 7 and 8.

When radio waves propagate through fluctuating charged-particle mediums, the amplitude and phase of the wave will fluctuate. If the rapid phase changes of a radio wave can be tracked and recorded, then the fluctuations of the total electron content along a raypath can be determined.

After the first Mercury encounter, once the SEP angle became less than 27 deg, there was strong evidence that the S-band doppler radio transmission was being phase-scintillated by plasma fluctuations. The S-band rms noise was now typically $\sim$0.04 Hz (10 times nominal). Superimposed on the 0.04-Hz rms noise background were frequent noise increases where in some instances the rms noise doubled (Fig. 1).

The X-band doppler rms noise was 6 to 20 times higher than the S-band doppler noise at $SEP \approx 27$ deg. If the X- and S-band radio waves were phase-scintillated as a result of charged-particle fluctuations, the X-band noise should be $(3/11)^2$ of the S-band noise except for the multiplication of (11/3) before scintillation. Thus, either the S- and X-band propagations, or both, were exhibiting noise that was not a direct measure of charged-particle dynamics.

Spacecraft radio tracking systems employ second-order phase-lock-loop electronics (Ref. 8). Both ground and spacecraft receivers do. Such loops require less than $\pi/2$ radians of phase coherence over time scales of a second. $\pi/2$ radians of phase scintillation translates to $\sim$3.5 cm of S-band doppler phase jitter or electron content fluctuations of 5×10^{15} electrons/m^2 along the raypath. When such plasma fluctuations do occur, then the S-band phase jitter may exceed the performance limitations of second-order phase-lock-loop receivers. Thus, cycle slips may be introduced into the doppler data stream.

However, it will be remembered that the X-band propagation was obtained at the spacecraft by multiplying the received uplink S-band carrier by 880/221. Thus, the phase jitter of the S-band uplink radio wave is also multiplied by 880/221. The X-band radio wave transmitted from the spacecraft has ~ 4 times more phase jitter than did the spacecraft S-band signal.

D. L. Brunn of JPL has shown that if the spacecraft-received S-band carrier has an rms phase jitter of $\sim \pi/6$ radians, the resultant X-band signal transmitted from the spacecraft will appear non-coherent to the DSS second-order phase-lock-loop receiver. This conclusion was based on laboratory measurements.

Mariner 10 telemetry data indicate that the rms phase jitter of the spacecraft-received S-band carrier was $\pi/12$ radians or less for the range of SEP angle of 30 deg down to 10 deg. And, undoubtedly, the statistical properties of the plasma dynamics as a doppler noise generator differ appreciably from those used in the laboratory. Thus, the X-band phase jitter being greater than the S-band phase jitter means

(1) Four times the phase jitter of the spacecraft-received S-band carrier exceeds the round-trip S-band carrier phase jitter, and, perhaps that

(2) Four times the phase jitter of the spacecraft-received S-band carrier is beyond the ability of second-order phase loops to track coherently.

Assume that the plasma dynamics encountered by the DSS-to-spacecraft uplink S-band transmission is also encountered on the downlink S-band transmission. Then the round-trip phase jitter on the S-band carrier is 2 or $\sqrt{2}$ times the one-way phase jitter, depending if statistical independence is assumed or not. The phase jitter of the X-band carrier is 4 times the one-way S-band phase jitter. Thus, the ratio X-band phase jitter to S-band phase jitter cannot exceed 4 if plasma dynamics constitute the sole source of the jitter. A relative noise pattern of S- and X-band, 60-s doppler is shown in Fig. 9.

When S/X dual-frequency doppler calibrations are computed using Eq. (3), the calibrations exhibit noise similar to the X-band doppler noise, the relationship being

$$\sigma_c \approx \sqrt{\sigma_x^2 + \sigma_s^2}$$

When S-band doppler is calibrated for plasma effects, the calibrated S-band doppler then exhibits noise similar to the X-band doppler noise (Fig. 10). If the calibrations are averaged over 20 minutes, the phase jitter is reduced an order of magnitude (Fig. 11), but the resultant time history of the plasma fluctuation over the view period is

not consistent with the S-band doppler structures assumed to the result of plasma dynamics (Fig. 10). When S/X dual-frequency calibrations are applied to the orbit determination process, the estimate of the Mariner 10–Mercury II encounter position is in error by $\sim$ 10,000 km. When uncalibrated doppler is used in the ODP, the position estimate for the second Mercury encounter has only a 170-km error. Obviously, these calibrations are erroneous for these high plasma dynamics.

Root mean square doppler noise, as indicated in Fig. 1, represents a major problem to deep space navigation. The Mariner Venus–Mercury 1973 Orbit Determination Team used such "noisy" doppler to predict the second Mercury encounter, target-plane encounter coordinates of the Mariner 10 spacecraft. Tracking data arcs (of extremely edited doppler) from 3 days to months in length were "fit" to the probe state. Although the scatter of these predictions was 800 km (σ) in the Mercury target plane, the "mean adopted" prediction was only 170 km removed from the *a posteriori* encounter position. The large scatter stems, in the main, from the continuous high and variable intensity of the "unmodeled" plasma dynamics. Using tracking data arcs of the same time duration prior to the third Mercury encounter when the doppler revealed little evidence of plasma effects, the spread in the third encounter target plane coordinate estimates was < 70 km (σ), an order of magnitude less.

VI. Viking 1975 S/X Dual-Frequency Plans

The next opportunity to evaluate S/X dual-frequency calibrations for the influence of charged particles on S-band doppler will be during the Viking 1975 mission. During the cruise and Mars orbital phases of that mission, S/X dual-doppler, S/X dual-range, differenced range versus integrated doppler, and S-band doppler integrated phase will be compared. The time histories of the plasma dynamics will be compared to ascertain at what level of plasma dynamics inconsistencies, if any, occur.

The S- and X-band doppler will be tracked by second-order phase-lock-loop receivers during the Viking mission. Additionally, the Viking Radio Science Team plans to record S- and X-band signals following the last mixers (before the signals enter the second-order phase-lock loops). The recorded bandwidths are tenths of kilohertz wide. Digital computer programs will then reduce two data streams to differential measurements of dispersive doppler shifts. This information will be compared to the differential measurements derived from the phase-lock-loop circuitry for consistency. It is hoped that these comparisons can be made over a spread of Sun–Earth–probe angle and plasma dynamics to determine under what plasma conditions the conventional tracking system yields valid S/X dual-frequency charged-particle calibrations.

The Radio Science Team has plans to develop power spectra for the phase and amplitude variations that are computed by the team's computer programs. As often as practical, S- and X-band doppler will be acquired at high sample rates (10 points/second) and autocorrelation processes will be used to develop a power spectra of the second phase-lock-loop differential measurements. The relative consistencies of the periodic natures and power distributions of the two will be examined.

VII. Conclusion

Doppler rms noise increases orders of magnitude as the Sun–Earth–probe angle changes from 30 to 3 deg for spacecraft at a distance greater than 1 AU from Earth.

S/X dual-frequency doppler data can yield valid charged-particle calibrations if the plasma fluctuations do produce S-band phase jitter near $\pi/12$ radians. At phase jitter levels higher than $\pi/12$ radians, valid calibrations may perhaps still be derived from S- and X-band doppler. However, for Mariner 10, once the angular separation between the probe and Sun as seen from Earth became less than 27 deg, S/X dual-frequency doppler did not yield valid charged-particle calibrations. The rms noise and signatures seen in the S- and X-band doppler are *not* a direct measure of plasma dynamics but the detection of them.

Although Mariner 10 long trajectory arcs of doppler were sufficiently stable to permit adequate navigation, order of magnitude uncertainties were introduced into the navigation for the second encounter with Mercury.

References

1. Moyer, T. D., *Mathematical Formulation of the Double-Precision Orbit Determination Program (DPODP),"* Technical Report 32-1527, Jet Propulsion Laboratory, Pasadena, Calif., May 15, 1971.

2. MacDoran, P. F., Callahan, P. S., and Zygielbaum, A. I., "Probing the Solar Plasma With Mariner Radio Metric Data, Preliminary Results," in *The Deep Space Network Progress Report,* Technical Report 32-1526, Vol. I, pp. 14–21, Jet Propulsion Laboratory, Pasadena, Calif., Feb. 15, 1971.

3. Muhleman, D. W., "A Measurement of the General Relativistic Time Delay with Data from Mariner 6 and 7," edited by R. W. Davies, *Proceedings of the Conference on Experimental Tests of Gravitation Theories,* California Institute of Technology, Pasadena, Calif., Nov. 11–13, 1970.

4. Berman, A. L., and Rockwell, S. T., "Correlation of Doppler Noise During Solar Conjunctions With Fluctuations in Solar Activity," in *The Deep Space Network Progress Report 42-30* (this volume), Jet Propulsion Laboratory, Pasadena, Calif., Dec. 15, 1975.

5. Esposito, P. B., *Helios—Investigation of Solar Corona and Relativistic Time Delays During Superior Conjunction,* EM 391-478, Aug. 22, 1973 (JPL internal document).

6. Laurence, R. S., et al., "A Survey of Ionospheric Effects Upon Earth-Space Radio Propagation," *Proc. IEEE,* Jan. 1964.

7. Winn, F. B., et al., *S/X Dual-Frequency Demonstration,* EM 391-582, July 11, 1974 (JPL internal document). Also available in AIAA Paper 74-832, presented at the AIAA Mechanics and Control of Flight Conference, Anaheim, Calif., Aug. 5–9, 1974.

8. Gardner, F. M., *Phaselock Techniques,* John Wiley & Sons, Inc., New York, 1966.

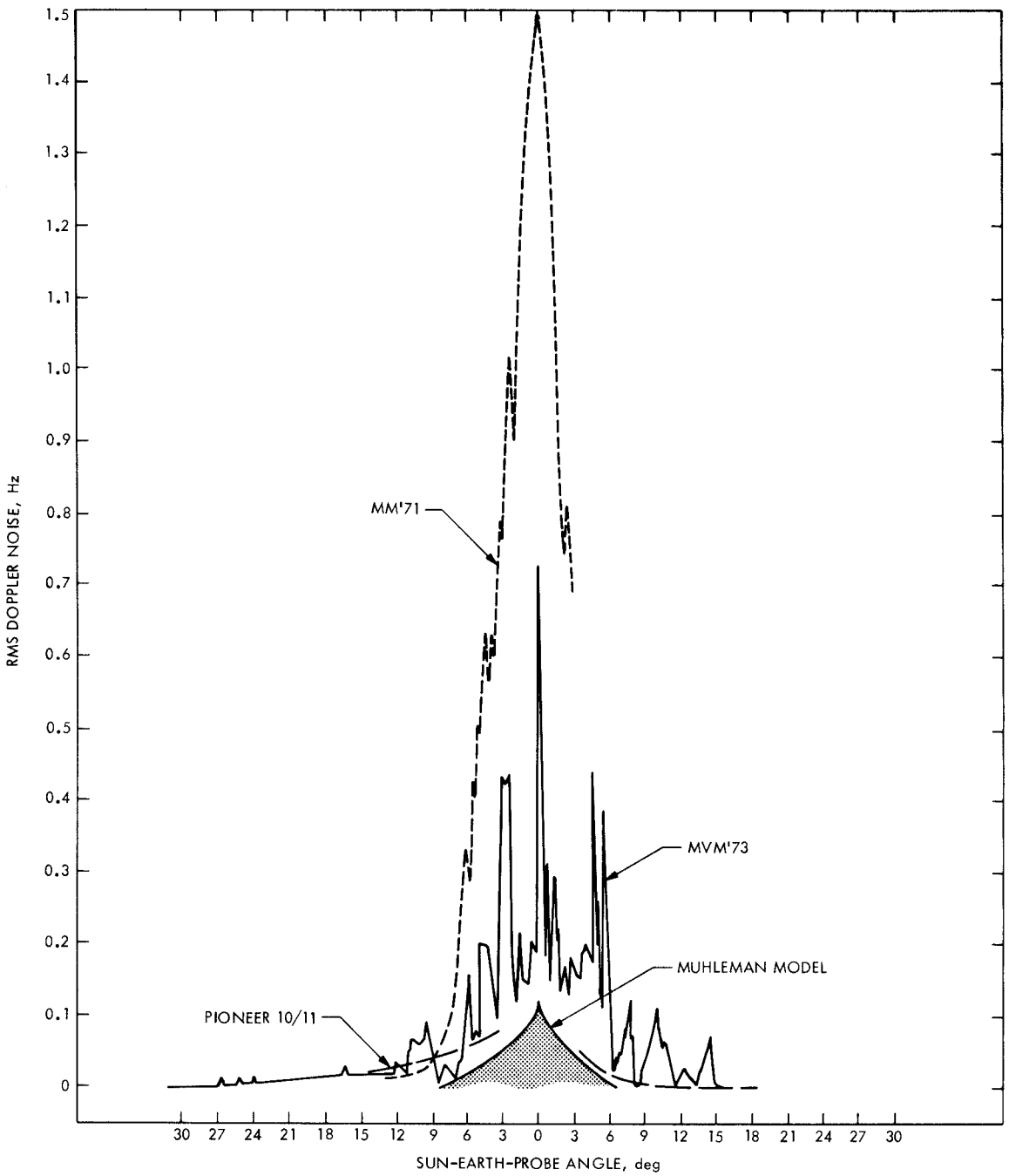

Fig. 1. RMS doppler noise vs Sun-Earth-probe angle

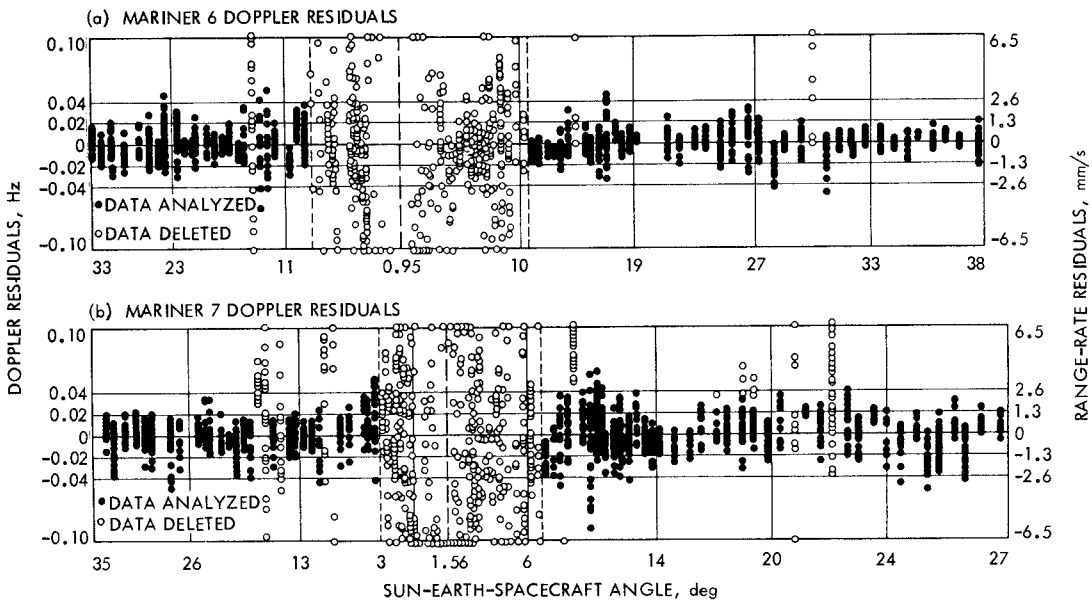

Fig. 2. Mariner 6 and 7 doppler residuals

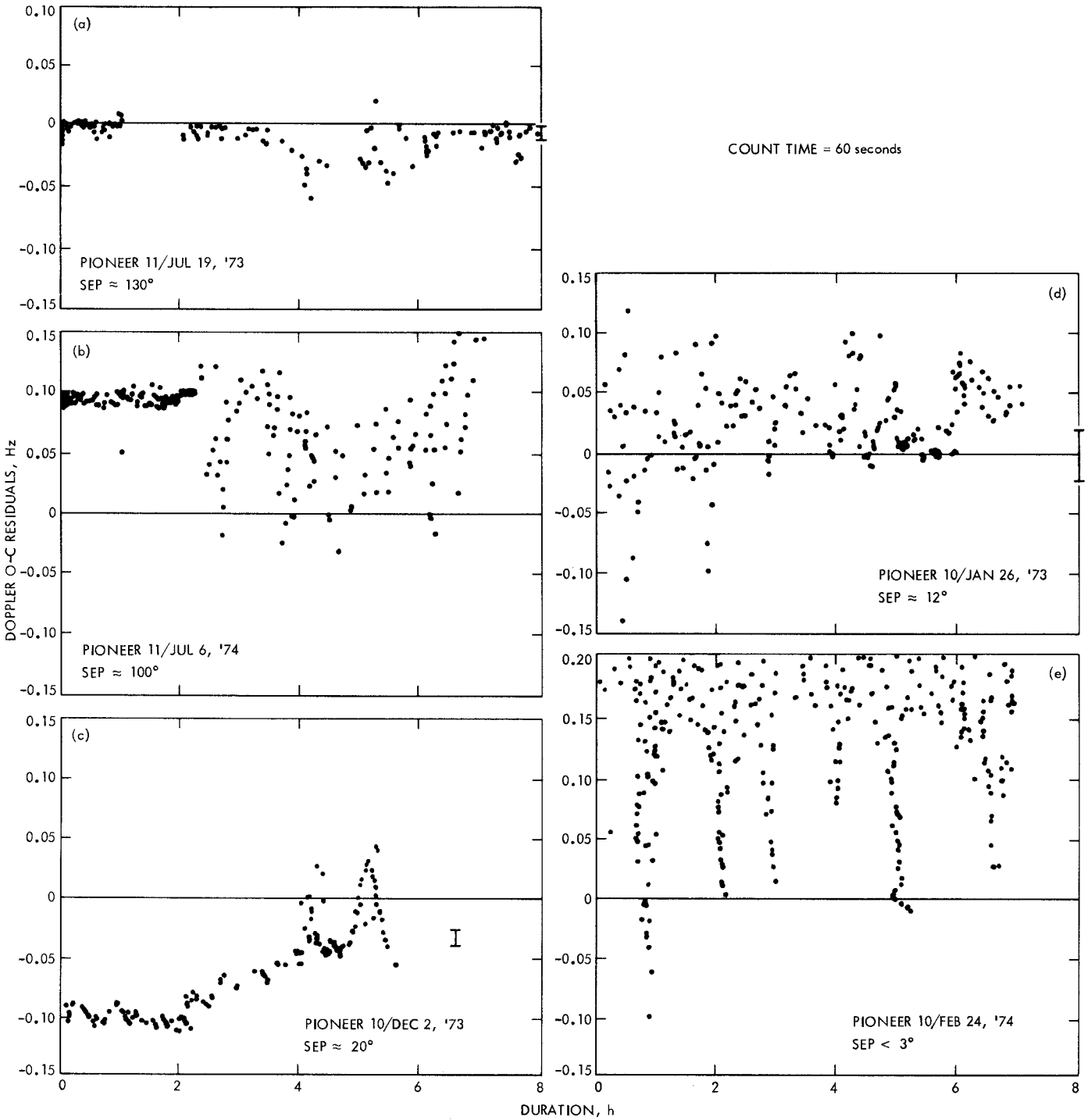

Fig. 3. Pictorials of Pioneer 10 and 11 doppler residuals

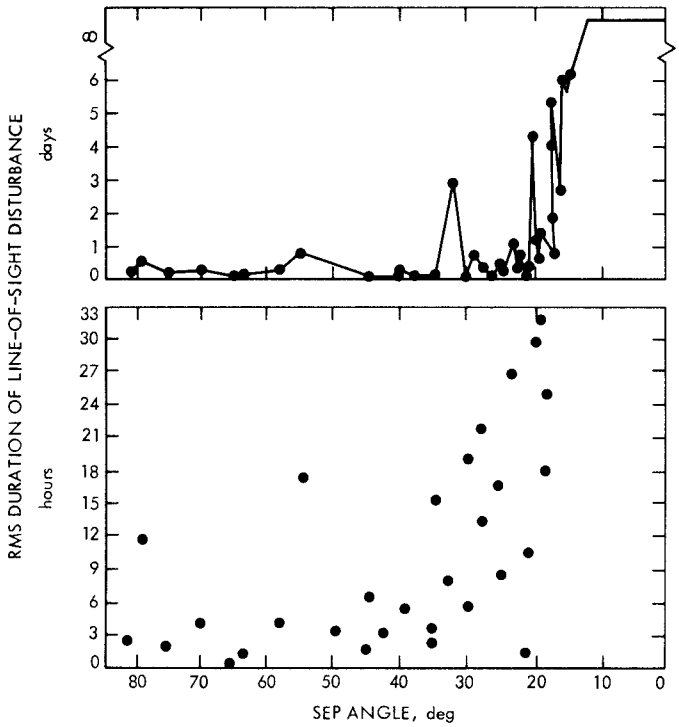

Fig. 4. Time duration of doppler degradation for Mariners 6, 7, and 10 and Pioneers 10 and 11

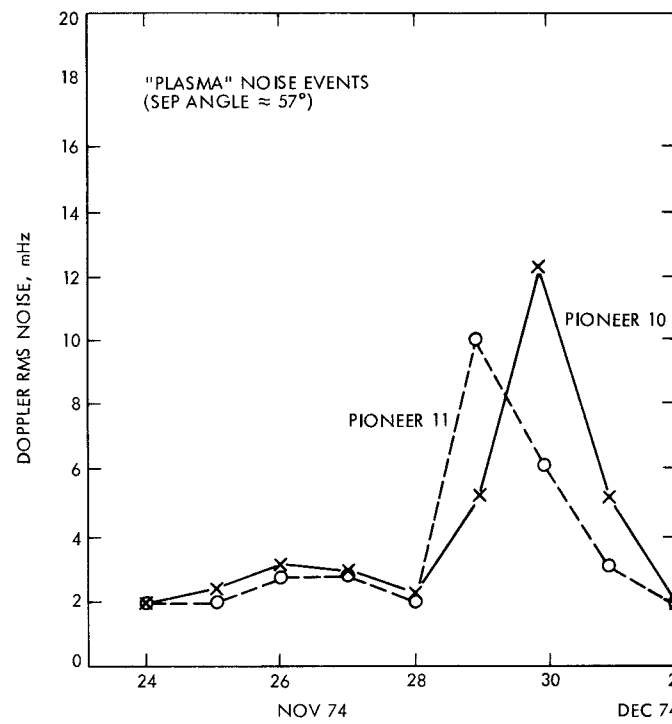

Fig. 5. Pioneer 10/11 time-correlated doppler degradations

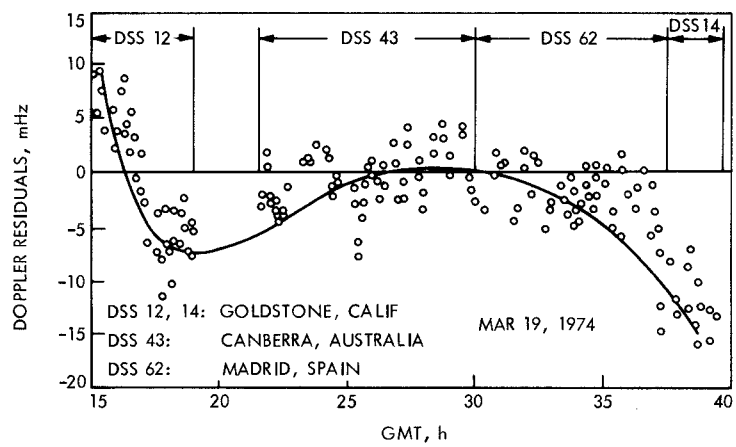

Fig. 6. Mercury I approach doppler noise patterns

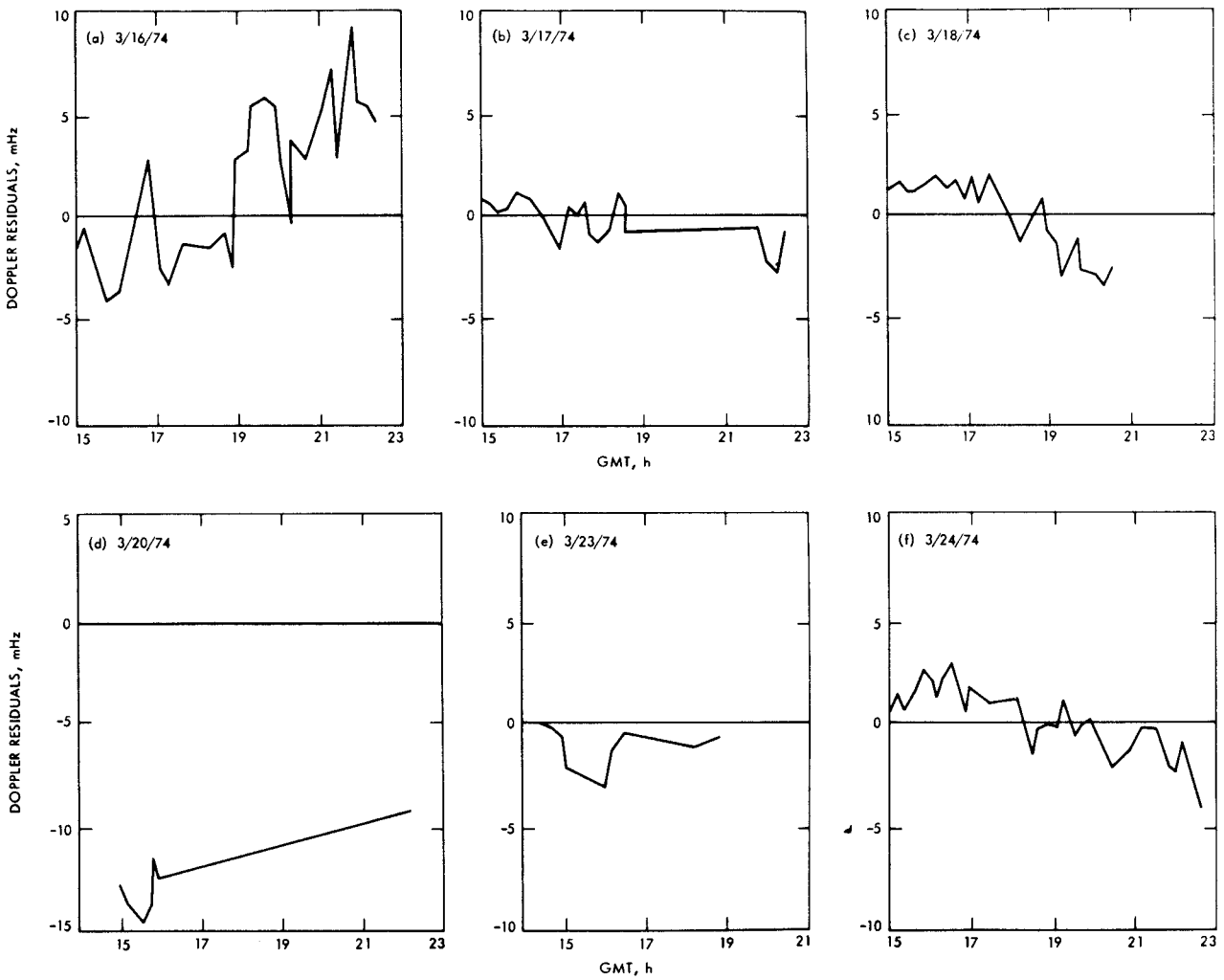

Fig. 7. S-band doppler residuals (600-s count time; no charged-particle calibrations) for Mariner 10-Mercury I encounter (residuals joined by line segments to aid viewing)

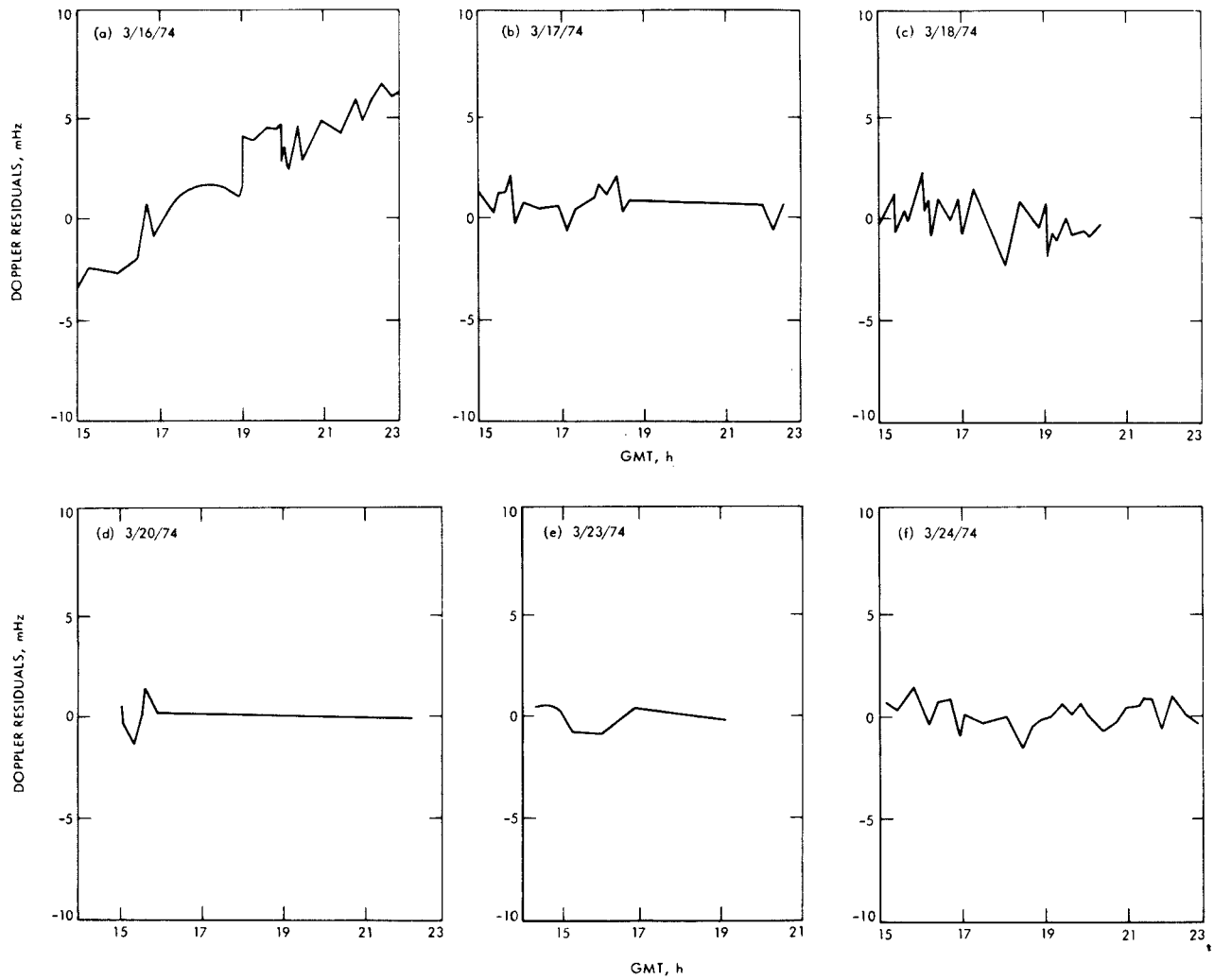

Fig. 8. Calibrated doppler residuals for Mariner 10-Mercury I encounter

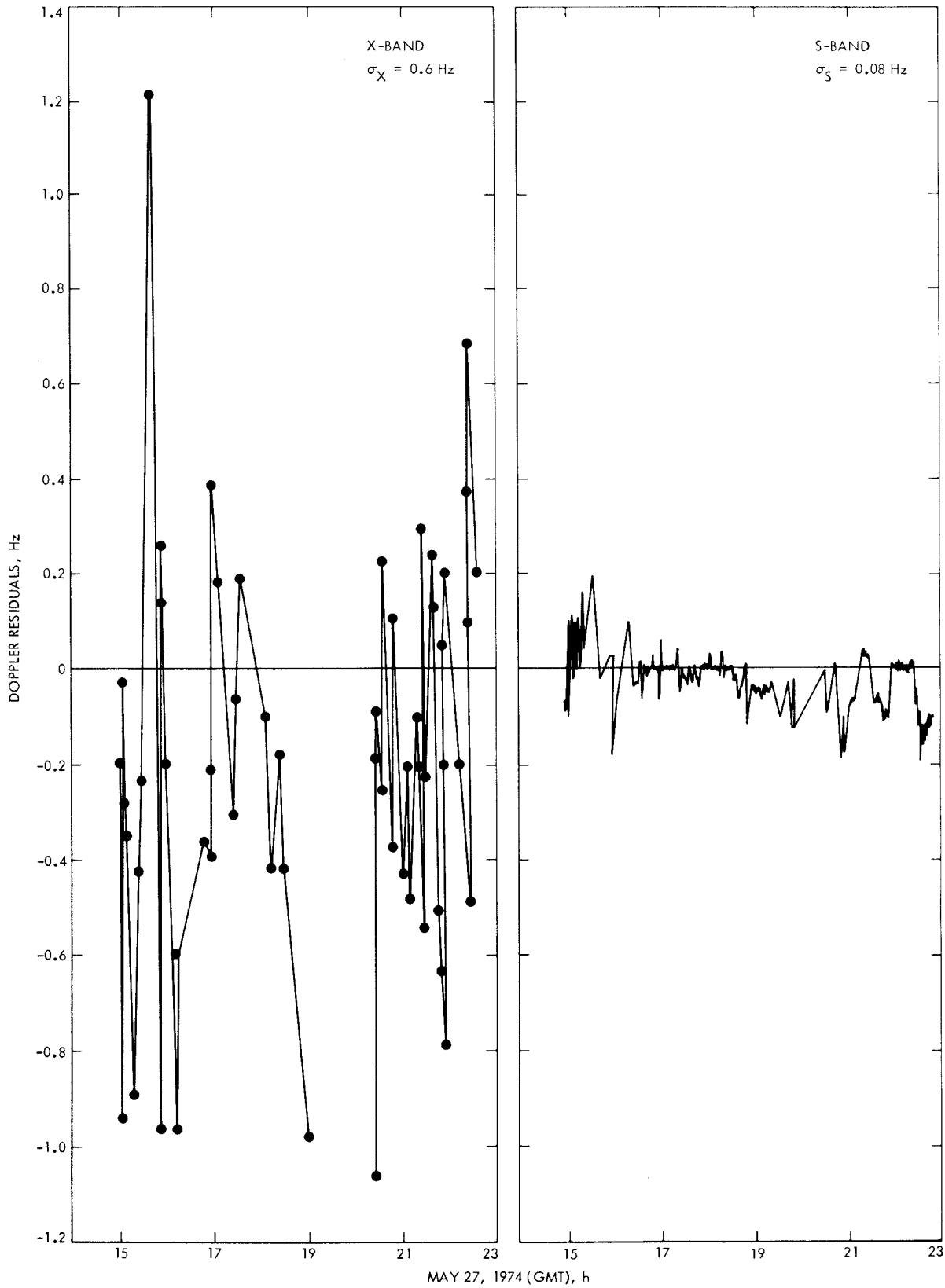

Fig. 9. Relative noise of X- and S-band doppler residuals

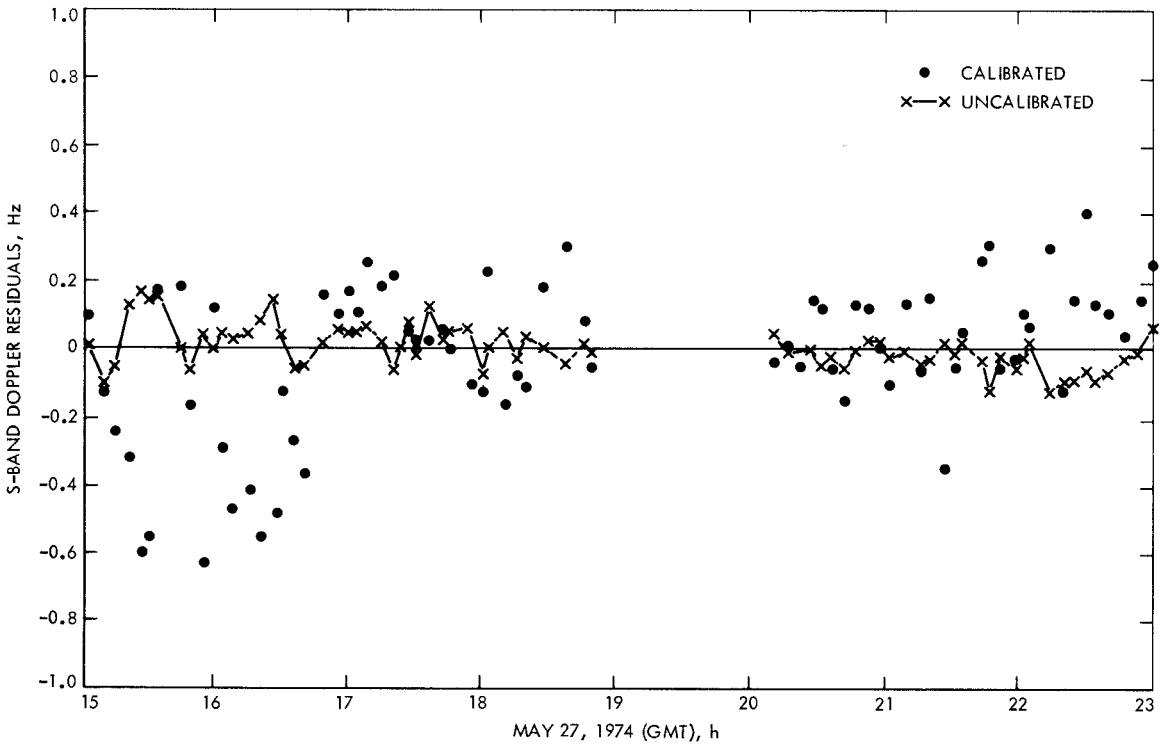

Fig. 10. Calibrated and uncalibrated S-band tracking doppler residuals

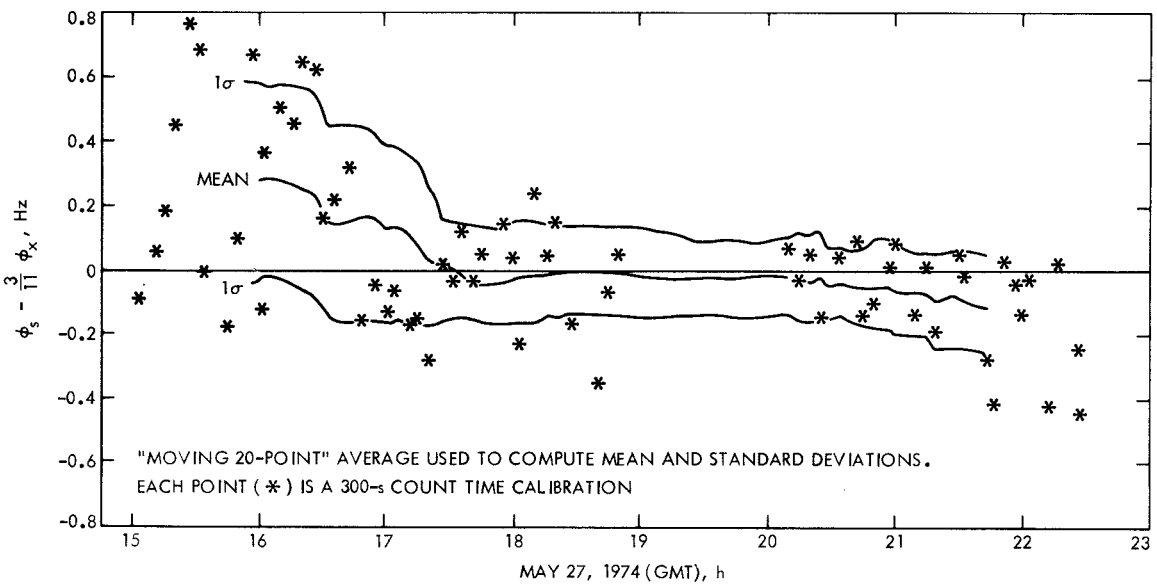

Fig. 11. S/X dual-doppler charged-particle calibration